Generation and characterization of multimode quantum frequency combs

Olivier Pinel, Pu Jian, Renné Medeiros de Araujo, Jingxia Feng, Benoît Chalopin, Claude Fabre, Nicolas Treps

Generation and Characterization of Multimode Quantum Frequency Combs

Olivier Pinel,[1] Pu Jian,[1] Renné Medeiros de Araújo,[1] Jingxia Feng,[1] Benoît Chalopin,[1,2] Claude Fabre,[1,*] and Nicolas Treps[1]

[1] *Laboratoire Kastler Brossel, Université Pierre et Marie Curie–Paris 6, ENS, CNRS; 4 place Jussieu, 75252 Paris, France*

[2] *Max Planck Institute for the Science of Light, Universität Erlangen-Nürnberg, IOIP, Staudtstrasse 7/B2, 91058 Erlangen, Germany*

(Dated: March 30, 2011)

Multimode nonclassical states of light are an essential resource in quantum computation with continuous variables [1], for example in cluster state computation [2, 3]. They can be generated either by mixing different squeezed light sources using linear optical operations [4], or directly in a multimode optical device [5, 6]. In parallel, frequency combs are perfect tools for high precision metrological applications [7, 8] and for quantum time transfer [9]. Synchronously Pumped Optical Parametric Oscillators (SPOPOs) have been theoretically shown to produce multimode non-classical frequency combs [10]. In this paper, we present the first experimental generation and characterization of a femtosecond quantum frequency comb generated by a SPOPO. In particular, we give the experimental evidence of the multimode nature of the generated quantum state and, by studying the spectral noise distribution of this state, we show that at least three nonclassical independent modes are required to describe it.

The generation of multimode nonclassical states in continuous variables is mostly done from the linear mixing of distinct Gaussian squeezed beams [11]. However, the difficulty of the experimental implementation of these schemes increases as the number of modes, i.e. the number of quantum resources, increases. Therefore it is interesting to explore the alternative technique, which is to use a single multimode source to produce nonclassical resources shared between several modes within a same beam: up to now, bipartite entangled spatial modes have been generated using a single OPO [6], a squeezed spatial tri-mode state has been produced by an OPO above threshold [5], and multimode squeezed solitons have been produced using an optical fibre [12].

Quantum frequency combs, which span over thousands of different frequency modes, have been proven to be good candidates for scalable generation of cluster states [13] and to be a powerful resource for precision measurements and parameter estimations [9, 14] below the standard quantum limit. The modes of the system can be described either in the temporal domain as trains of pulses having different temporal profiles, or in the frequency domain as frequency combs having different spectral profiles. Single-mode quantum noise reduction in frequency combs has already been achieved with femtosecond pulses usign optical fibre Kerr non-linearity [15], or with picosecond pulses in a SPOPO [16]. A SPOPO [17–19] is an OPO pumped by a train of ultrashort pulses that are synchronized with the pulses making round-trips inside the optical cavity. In our experiment, the frequency comb is produced by a singly-resonant SPOPO pumped with pulses in the femtosecond range, which are described in the frequency domain by a superposition of at least 10^5 longitudinal modes of frequencies ω_n^p located around the carrier frequency $2\omega_0$ and equally spaced by a repetition rate ω_r: $\omega_n^p = 2\omega_0 + n\omega_r$.

This huge number of modes leads to a great complexity of the parametric down conversion process taking place in the intracavity nonlinear crystal. Indeed, each pumping frequency ω_n^p is coupled through phase matched parametric interaction to many pairs of cavity-resonant frequencies ω_ℓ^s and $\omega_{n-\ell}^s$, where $\omega_\ell^s = \omega_0 + \ell\omega_r$, since they satisfy $\omega_n^p = \omega_\ell^s + \omega_{n-\ell}^s$. However, it has been demonstrated [10] that this interaction can be much more easily described by a substantially reduced number of modes which are the eigenmodes of the nonlinear interaction, named supermodes. These are well-defined coherent superposition of longitudinal modes characterized by their spectral amplitude and phase profiles. The mode profiles of the supermodes in the frequency domain, or in the time domain, are predicted to be close to Hermite-Gaussian functions [10].

The experimental setup is shown in (Fig. 1) and described in detail in the Methods section. The SPOPO is seeded by 120 fs pulses at 795 nm with a repetition rate of 76 MHz produced by a Ti:Sapphire mode-locked laser. Its second harmonic at 397 nm is used to pump the 350 μm long intracavity BIBO crystal [20]. Above a threshold of typically ~ 50 mW the SPOPO generates a unique signal-idler frequency comb having the same mean frequency as the Ti:Sapph laser (degenerate configuration). Below threshold, we observe phase-sensitive amplification of the seed. We lock the relative phase between the seed and the pump in the deamplification regime. The state of the output light is evaluated using a two-port balanced detector: the sum of the photocurrent fluctuations represents the intensity fluctuations Δn^2 of the output beam, and the difference represents the standard-quantum-limited fluctuations of a beam of same power $\Delta n^2_{shot} = \langle n \rangle$. We measure up to a normalized intensity

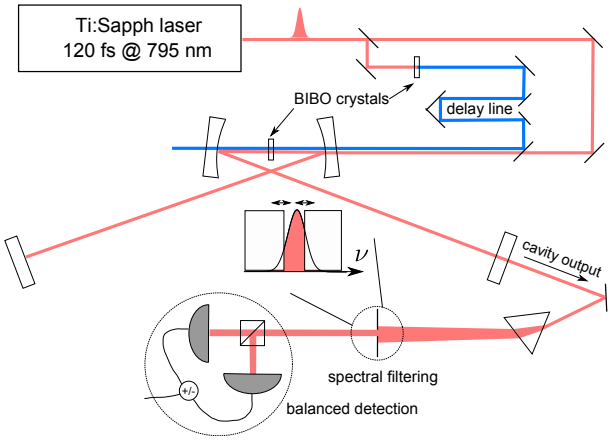

FIG. 1. **Schematic of the experimental setup.** The OPO is synchronously pumped by a frequency comb centered at 397 nm. The delay line ensures the temporal overlap between the pulses from the pump and seed at cavity input. At the cavity output, the deamplified frequency comb centred at 795nm is spectrally filtered. A balanced detection is used to measure the intensity noise: the shot noise level is yielded by the difference of photocurrents and the sum gives the signal noise of the beam.

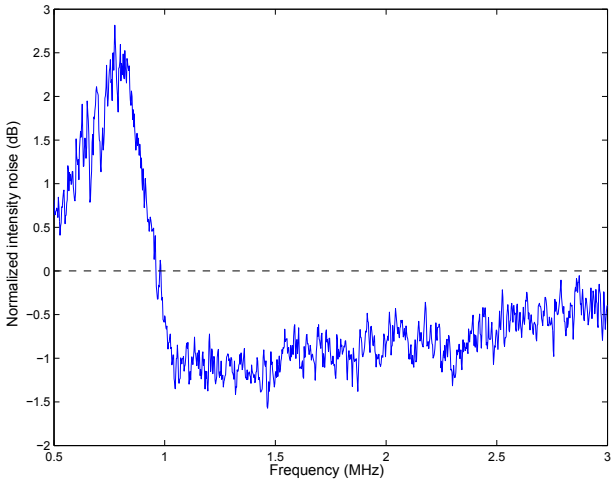

FIG. 2. **Spectral intensity noise (in dB) as a function of the analysis frequency on the spectrum analyzer.** The dashed line corresponds to the standard quantum limit. During this data acquisition, the phase modulations for the locking system were set at > 4 MHz. These data are not corrected from the electronic dark noise of the photodiodes. Resolution bandwidth: 30 kHz; video bandwidth: 10 Hz.

noise of $\frac{\Delta n^2}{\Delta n^2_{shot}} = 0.76 \pm 0.02$ at ~ 1.5 MHz, corresponding to 1.2 ± 0.1 dB of noise reduction on the amplitude quadrature (see Fig. 2). This experimentally demonstrates for the first time the non-classicality of the field generated by a femtosecond SPOPO below threshold. The low amount of squeezing may be explained by the fact that the seed is not optimized in the present status of the experiment: it does not coincide with the SPOPO supermode with highest achievable squeezing (later referred as the first supermode). Indeed the spectrum of this supermode, which depends on the spectrum of the pump and the length of the crystal, is theoretically 8.3 times broader than the spectrum of the seed. The field we measure with the balanced detection therefore corresponds to a superposition of different supermodes, which results in a higher intensity noise than in the first supermode. In addition, as the cavity frequency bandwidth at half maximum is 2.5 MHz, more squeezing should be observed at a lower noise frequency, which is presently not possible because of the presence of excess technical noise at low frequencies.

The multimode nature of the output beam was investigated by studying its noise distribution over the optical spectrum. The principle of this characterization is the spectral analogue of the technique used in [21–23] for spatially multimode quantum light. It consists in spectrally filtering the beam and studying the measured intensity noise as a function of the attenuation introduced by the filtering. Spectral filtering is done by spatially dispersing the frequencies of the output beam with two prisms, and then focusing it on a variable slit. This allows for low-, high- or bandpass filtering. The spectral resolution of the filter is 1.8 nm. For a single-mode beam, any filtering is equivalent to overall attenuation, so the normalized intensity noise of the beam is a linear function of the transmission, while for a multimode beam, the intensity noise may vary differently for different spectrum ranges. The multimode criterion can then be summarized as follows: if the normalized intensity noise is not linear as a function of the transmission, the beam is necessarily multimode [23, 24].

The results and the theoretical singlemode prediction are plotted in Fig. 3. One observes a good agreement between the experimental data obtained for overall attenuation and a linear fit, characteristic of the single mode case. The noise reduction is clearly smaller when the low frequencies are filtered than in a single-mode beam. In contrast, the results for high frequency filtering (not shown on Fig. 3 for clarity) have the same dependency as the theoretical single-mode case. The difference between low- and high- pass filtering implies that the frequency profiles of the eigenmodes of the output beam are not exactly symmetrical around the centre frequency of the spectrum.

In order to characterize precisely the mode content of our quantum frequency comb, we apply the experimental technique and data analysis method developed in [12, 25]. We describe this comb over a four "frequency pixels" basis, which are four consecutive wavelength intervals of equal intensity. We have recorded the actual intensity noise and the shot noise level for the 10 different frequency intervals obtained by combining adjacent pixels. For each interval formed by a sum

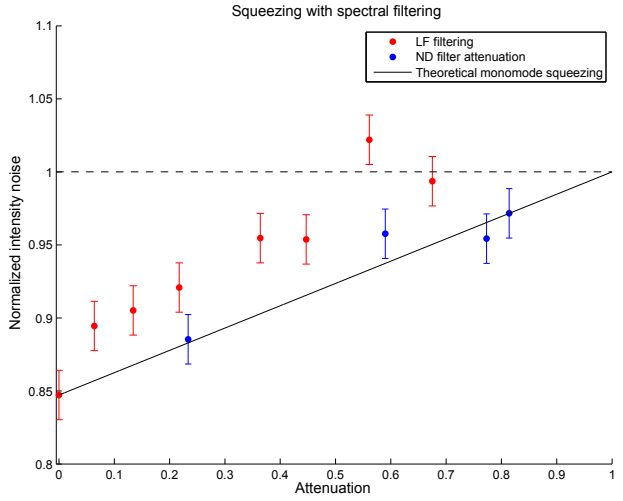

FIG. 3. **Normalized intensity noise as a function of the attenuation**. Experimental data points at 2.5 MHz for lowpass filtering (in red) and overall attenuation with neutral density filters(in blue); in solid line, the theoretical function for a single-mode beam.

of pixels $\{i_1, \ldots, i_m\}$, the detected intensity fluctuations are $\Delta\big(\sum_{i=i_1,\ldots,i_m} n_i\big)^2 = \sum_{i,j=i_1,\ldots,i_m} \mathrm{cov}(n_i, n_j)$ where $\mathrm{cov}(n_i, n_j) = \langle n_i n_j\rangle - \langle n_i\rangle\langle n_j\rangle$ is the photon number covariance. From these measurements, the intensity correlation matrix can be reconstructed and is plotted in Fig. 4.

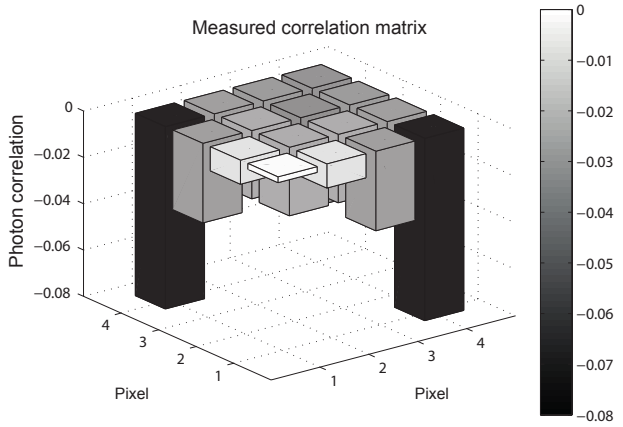

FIG. 4. **Normalized photon number correlation matrix as a function of the spectral pixels:** $C(i,j) = \frac{\mathbf{cov}(n_i,n_j)}{\sqrt{\Delta n_i^2 \Delta n_j^2}} - \delta_{ij}\frac{\Delta n_{i,shot}^2}{\Delta n_i^2}$**.** As the pixels have the same power, in the single-mode case, all the correlation should be equal. The presence of one diagonal element with less local squeezing and of one off-diagonal element with more anti-correlation than the other coefficients is specific to a multimode field.

This information can then be used to reconstruct the covariance matrix in the pixel basis :

$$V_{x_i,x_j} = \frac{1}{2}\langle \delta x_i \delta x_j + \delta x_j \delta x_i\rangle \qquad (1)$$

where $x_i = a_i + a_i^\dagger$ is the amplitude quadrature, and $\delta x = x - \langle x\rangle$. The phase quadrature information cannot be recovered from our technique as we measure only amplitude fluctuations. Thus, we assume that the different frequency components of the output field have the same phase, and can all be taken as real. Using the derivation discussed in [25], one finds $\mathrm{cov}(n_i, n_j) \approx \langle x_i\rangle\langle x_j\rangle V_{x_i,x_j}$. The mean photon number in one pixel is taken as $\langle n_i\rangle \approx \langle x_i\rangle^2$, leading to the following expression for the elements of the covariance matrix:

$$V_{x_i,x_j} = \frac{\mathrm{cov}(n_i, n_j)}{\sqrt{\Delta n_{i,shot}^2 \Delta n_{j,shot}^2}} \qquad (2)$$

The diagonalisation of the covariance matrix V allows one to find a set of four independent modes (corresponding to the eigenvectors of V), together with their respective amplitude noise variances (corresponding to the eigenvalues of V). We find that among these four eigenmodes S_ℓ, two have eigenvalues smaller than the standard quantum limit 1, and one has an eigenvalue greater than 1, as shown in Fig. 5. The measurement noise does not allow us to conclude whether the fourth mode S_4 is excited (for details about the uncertainty estimation, see Methods). This shows that the output of the SPOPO is described by at least 3 independent modes, two of them at least being in a squeezed state.

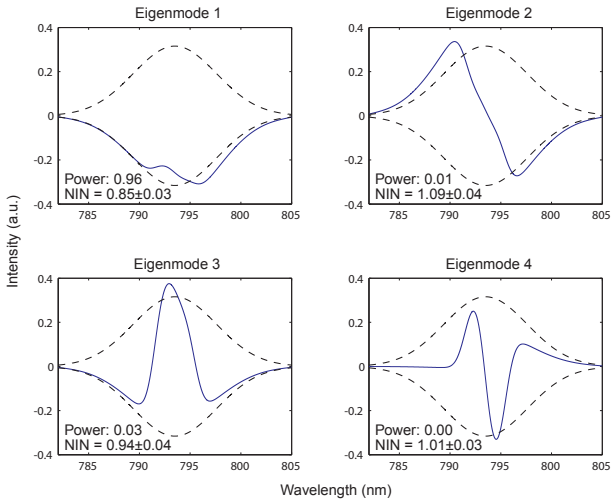

FIG. 5. **Wavelength profile of the eigenmodes S_ℓ.** The pixel modes are smoothed by taking into account the 1.8nm spectral resolution of the bandpass filters. The solid lines correspond to the supermodes; the dashed line corresponds to the mean field mode. Power: percentage in optical power of the output beam; NIN: normalized intensity noise.

Furthermore, the eigenmode S_1, within which lies most of the power of the light beam, has approximately the same amount of squeezing than the mean field. The spectrum of S_1 is slightly broader than the mean field mode, which is consistent with the theoretical prediction [10] for

the first supermode in our experimental conditions. We also observe that the profile of S_2 resembles a Hermite-Gaussian mode of order 1, and shows excess noise; this is also consistent with the theory, which predicts that the second supermode of the SPOPO is a first order Hermite-Gaussian mode squeezed in phase, and therefore anti-squeezed in amplitude. In the same way, the profile of eigenmodes S_3 appears like a Hermite-Gaussian mode of order 2, and S_3 is squeezed, as predicted by its even order. Finally, the slight asymmetry in theses modes explains the asymmetry in the low- and high-pass filtering experiment.

The procedure that we have described demonstrates that at least three orthogonal modes are necessary to describe the output field of the SPOPO, two being in squeezed states. However, a complete description of this field may involve more modes: separating the spectrum in more than four pixels may reveal intensity correlations which would require more than three modes to be described. Moreover, this derivation does not take into account the possibility of correlations with the phase fluctuations p_i. A complete characterization of the quantum state of the output of the SPOPO requires to have access to V_{p_i,p_j} and V_{x_i,p_j}. By shaping the local oscillator pulses [26] of a homodyne detection, one can directly measure the noise of an arbitrary mode on any quadrature.

In conclusion, we have experimentally demonstrated that femtosecond SPOPOs are able to generate multimode quantum frequency combs that can be precisely characterized and analyzed in terms of squeezed uncorrelated eigenmodes of experimentally determined shapes. The low level of noise reduction and of quantum correlation makes it so far a proof-of-principle experiment. Noise reduction, and therefore possible entanglement, can be certainly drastically increased to much higher levels by working at lower noise frequencies and seeding with the first supermode. In addition, the exact multimode quantum state of the generated light can be adjusted by controlling the pump pulse shape and duration. This experiment therefore opens the way to the production of quantum frequency combs that are tailored to fit the requirements of its numerous applications in quantum information processing and quantum metrology.

METHODS

Experimental apparatus

The Ti:Sapphire mode-locked laser used in the experiment is a Coherent Mira-900, pumped by a Coherent Verdi V-18. It produces pulses at a repetition rate of 76 MHz. The pulses are centred at 795 nm with a spectral width of 7 nm (FWHM) and a pulse duration of $\sim$ 120 fs (FWHM). This source is used to produce a strong field at 397 nm by frequency doubling in a 200 μm long BIBO crystal, pumping a linear SPOPO. The optical cavity has a finesse of ~ 28 for the signal and is not resonant for the pump; the BIBO crystal inside has a length of 350 μm. The SPOPO is seeded with a 795 nm field. Temporal overlap between the pulses of the seed and the intracavity seed is ensured by a delay line on the path of the pump before the cavity. While sweeping the relative phase between the pump and the seed, we observe the phase dependent amplification regime. While the phase is locked on the deamplification regime, we typically observe a de-amplification gain of ~ 0.5. Both the cavity length and the relative phase between the pump and the seed are locked using a small extracted fraction of the cavity output power ($< 5\%$) and the error signal is obtained through the Pound-Drever-Hall technique with piezo-induced phase modulations. The detectors used in the balanced detection have a quantum efficiency above 90 %; we achieve more than 30 dB noise extinction between the two detectors.

The spectral filtering system consists in: two lenses for expanding the beam size at the output of the SPOPO (the spectral resolution of the system increases with the size of the beam); two SF10 prisms used at Brewster's angle; a spherical mirror of radius of curvature 50 cm that focuses the dispersed beam onto the variable slit; and another spherical mirror of same radius of curvature for re-collimating the beam before the detection apparatus. The whole filtering system introduces $\sim 10\%$ of loss.

The data presented in this paper are not corrected for these losses.

Uncertainty of filtered squeezing measurements

For the characterization of the multimode nature of the field produced by the SPOPO using low- and high-pass filtering, and ND filter attenuation, the following procedure is used to estimate the uncertainty of the measurements: for each position of the razor blade, we measure successively the intensity noise and the shot noise during 5 seconds, corresponding to 1 000 data points for each measurement. The SPOPO remains locked during all the measurement process. The mean values are used to calculate the normalized intensity noise for each position. For the calculation of the error bars, each set of 1 000 data points is split into two sets of 500 data points; using the mean values of these subsets, we obtain 4 estimations of the normalized intensity noise for each position of the razor blade. A common confidence interval for all positions of the razor blades is then defined as containing 95 % of the estimations of the normalized intensity noise.

Estimation of uncertainty in the eigenmode basis

Let us note O the orthogonal matrix of the eigenvectors of V components, and D the diagonal matrix corresponding to the eigenvalues of V, so that: $O^T V O = D$. In order to estimate the precision of the results on the eigenmodes, we use a Monte-Carlo approach and generate 10 000 correlation matrices $C^{(k)}$ ($k = 1, \ldots, 10\,000$) with elements randomly picked among our data points (1 000 data points for each measurement). We apply the basis change matrix O to the variance matrices $V^{(k)}$ derived from the $C^{(k)}$; this action corresponds to a 'pseudo-diagonalisation', or in more physical terms, to a measurement of the Monte-Carlo generated field corresponding to $C^{(k)}$ in the basis of the eigenmodes S_l. The off-diagonal elements of $D^{(k)} = O^T V^{(k)} O$ fluctuate around 0 ± 0.03, showing that the eigenmodes S_l are effectively eigenmodes of the Monte-Carlo generated fields. The normalized intensity noise of the eigenmode S_1 (respectively S_2, S_3 and S_4), given by the diagonal elements of $D^{(k)}$, is 0.85 ± 0.03 (respectively 1.09 ± 0.04, 0.94 ± 0.04 and 1.01 ± 0.03).

We acknowledge the financial support of the Future and Emerging Technologies (FET) programme within the Seventh Framework Programme for Research of the European Commission, under the FET-Open grant agreement HIDEAS, number FP7-ICT-221906; and of the ANR project QUALITIME.

* claude.fabre@upmc.fr

[1] Lloyd, S. & Braunstein, S.L. Quantum computation over continuous variables. *Phys. Rev. Lett.* **82**, 1784 (1999).

[2] Zhang, J. & Braunstein, S.L. Continuous-variable Gaussian analog of cluster states. *Phys. Rev. A* **73**, 32318 (2006).

[3] Menicucci, N.C. *et al.* Universal quantum computation with continuous-variable cluster states. *Phys. Rev. Lett.* **97**, 110501 (2006).

[4] O'Brien, J.L., Furusawa, A., & Vučković, J.. Photonic quantum technologies. *Nature Photonics* **3**, 687 (2009).

[5] Chalopin, B., Scazza, F., Fabre, C. & Treps, N. Multimode nonclassical light generation through the optical-parametric-oscillator threshold. *Physical Review A* **81**, 61804 (2010).

[6] Janousek, J. *et al.* Optical entanglement of co-propagating modes. *Nature Photonics* **3**, 399 (2009).

[7] Holzwarth, R. *et al.* Optical frequency synthesizer for precision spectroscopy. *Phys. Rev. Lett.* **85**, 2264 (2000).

[8] Udem, Th., Holzwarth, R., & Hänsch, T. W. Optical frequency metrology. *Nature* **416**, 233 (2002).

[9] Lamine, B., Fabre, C. & Treps, N. Quantum improvement of time transfer between remote clocks. *Phys. Rev. Lett.* **101**, 123601 (2008).

[10] Patera, G., Treps, N., Fabre, C. & De Valcarcel, G.J. Quantum theory of Synchronously Pumped type I Optical Parametric Oscillators: characterization of the squeezed supermodes. *The European Physical Journal D* **56**, 123 (2009).

[11] Yukawa, M., Ukai, R., Van Loock, P. & Furusawa, A. Experimental generation of four-mode continuous-variable cluster states. *Phys. Rev. A* **78**, 12301 (2008).

[12] Spälter, S., Korolkova, N., König, F., Sizmann, A. & Leuchs, G. Observation of multimode quantum correlations in fiber optical solitons. *Phys. Rev. Lett.* **81**, 786 (1998).

[13] Menicucci, N.C., Flammia, S.T., & Pfister, O. One-way quantum computing in the optical frequency comb. *Phys. Rev. Lett.* **101**, 130501 (2008).

[14] Pinel, O., Fade, J., & Treps, N. General Cramér-Rao bound for parameter estimation using Gaussian multimode quantum resources. Preprint at ¡http://arXiv:1008.0844v1¿ (2010).

[15] Spälter, S. *et al.* Photon number squeezing of spectrally filtered sub-picosecond optical solitons. *Europhys. Lett.* **38**, 335 (1997).

[16] Shelby, R.M. & Rosenbluh, M. Generation of pulsed squeezed light in a mode-locked optical parametric oscillator. *App. Phys. B: Lasers and Optics* **55**, 226 (1992).

[17] Cheung, E.C. & Liu, L.M. Theory of a synchronously pumped optical parametric oscillator in steady-state operation. *J. Opt. Soc. Am. B* (7), 1385 (1990).

[18] Edelstein, D.C., Wachman E.S. & Tang, C.L. Broadly tunable high repetition rate femtosecond optical parametric oscillator. *Appl. Phys. Lett.* **54**, 1728 (1989).

[19] Van Driel, H.M. Synchronously pumped optical parametric oscillators. *App. Phys. B: Lasers and Optics* **60**, 411 (1995).

[20] Hellwig, H., Liebertz, J. & Bohatý, L. Exceptional large nonlinear optical coefficients in the monoclinic bismuth borate BiB_3O_6 (BIBO). *Solid State Commun.*, **109**, 4 (1998)

[21] Poizat, J.P., Chang, T., Ripoll, O. & Grangier, P. Spatial quantum noise of laser diodes. *J. Opt. Soc. Am. B* **15**, 1757 (1998).

[22] Hermier, J.P. *et al.* Spatial quantum noise of semiconductor lasers. *J. Opt. Soc. Am. B* **16**, 2140 (1999).

[23] Martinelli, M. *et al.* Experimental study of the spatial distribution of quantum correlations in a confocal optical parametric oscillator. *Phys. Rev. A* **67**, 23808 (2003).

[24] Treps, N., Delaubert, V., Maître, A., Courty, J.M. & Fabre, C. Quantum noise in multipixel image processing. *Phys. Rev. A* **71**, 13820 (2005).

[25] Opatrný, T., Korolkova, N. & Leuchs, G. Mode structure and photon number correlations in squeezed quantum pulses. *Phys. Rev. A* **66**, 53813 (2002).

[26] Cundiff, S.T. & Weiner, A.M. Optical arbitrary waveform generation. *Nature Photonics* **4**, 760 (2010).